Universal scaling laws and density slope for dark matter halos from rotation curves and energy cascade

Zhijie (Jay) Xu,[1]⋆

[1]*Physical and Computational Sciences Directorate, Pacific Northwest National Laboratory; Richland, WA 99352, USA*

ABSTRACT

Smalls scale challenges suggest some missing pieces in our current understandings of dark matter. A cascade theory for dark matter flow is proposed to provide extra insights, similar to the cascade in hydrodynamic turbulence. The energy cascade from small to large scales with a constant rate ε_u ($\approx -4.6 \times 10^{-7} m^2/s^3$) is a fundamental feature of dark matter flow. Energy cascade leads to a two-thirds law for kinetic energy v_r^2 on scale r such that $v_r^2 \propto (\varepsilon_u r)^{2/3}$, as confirmed by N-body simulations. This is equivalent to a four-thirds law for mean halo density ρ_s enclosed in the scale radius r_s such that $\rho_s \propto \varepsilon_u^{2/3} G^{-1} r_s^{-4/3}$, as confirmed by data from galaxy rotation curves. By identifying relevant key constants, critical scales of dark matter might be obtained. The largest halo scale r_l can be determined by $-u_0^3/\varepsilon_u$, where u_0 is the velocity dispersion. The smallest scale r_η is dependent on the nature of dark matter. For collisionless dark matter, $r_\eta \propto (-G\hbar/\varepsilon_u)^{1/3} \approx 10^{-13} m$, where $\hbar$ is the Planck constant. A uncertainty principle for momentum and acceleration fluctuations is also postulated. For self-interacting dark matter, $r_\eta \propto \varepsilon_u^2 G^{-3} (\sigma/m)^3$, where σ/m is the cross-section. On halo scale, the energy cascade leads to an asymptotic slope $\gamma = -4/3$ for fully virialized halos with a vanishing radial flow, which might explain the nearly universal halo density. Based on continuity equation, halo density is analytically shown to be closely dependent on the radial flow and mass accretion such that simulated halos can have different limiting slopes. A modified Einasto density profile is proposed accordingly.

Key words: Dark matter flow; N-body simulations; Rotation curve; Collisionless; Self-interacting; Core-cusp

CONTENTS

1 INTRODUCTION

Standard CDM (cold dark matter) paradigm of cosmology has many successes in the formation and evolution of large scale structures and the contents and states of our universe (Peebles 1984; Spergel et al. 2003; Komatsu et al. 2011; Frenk & White 2012). Despite great successes, serious theoretical and observational difficulties still exist (Perivolaropoulos & Skara 2022; Bullock & Boylan-Kolchin 2017). Especially, CDM model predictions of structures on small scales (<1Mpc) are inconsistent with some observations. Examples are the core-cusp problem (Flores & Primack 1994; de Blok 2010), the missing satellite problem (Klypin et al. 1999; Moore et al. 1999), the too-big-to-fail problem (Boylan-Kolchin et al. 2011, 2012). In addition, the origin of Baryonic Tully-Fishser relation (BTFR) and MOND (modified Newtonian dynamics) (Milgrom 1983; McGaugh et al. 2000; Famaey & McGaugh 2013) is still not clear.

These smalls scale challenges might be related to each other

(Garrison-Kimmel et al. 2014; Bullock & Boylan-Kolchin 2017; Del Popolo et al. 2014) and suggest missing pieces in our current understandings. First, the cusp-core problem describes the discrepancy between the cuspy halo density predicted by cosmological CDM only N-body simulations and the cored density inferred from observational data for dwarf galaxies. The predicted halo density exhibits a cuspy profile with inner density $\rho(r) \propto r^\gamma$, where slope γ persistently exceeds different observations (de Blok & Bosma 2002; de Blok et al. 2003; Swaters et al. 2003; Kuzio de Naray & Kaufmann 2011). Even for the cuspy profile predicted by cosmological simulations, there seems no consensus on the exact value of asymptotic slope γ, but with a wide range between -1.0 to -1.5. Since the first prediction of $\gamma = -1.0$ in NFW profile (Navarro et al. 1997), the inner density slope of simulated halos seems to have different values from $\gamma > -1.0$ (Navarro et al. 2010) to $\gamma = -1.2$ (Diemand & Moore 2011), and $\gamma = -1.3$ (Governato et al. 2010; McKeown et al. 2022). To summarize, some key questions are: is there an asymptotic slope for dark matter halos? why there exists a nearly universal density profile? and why different inner slopes γ exist in simulations?

The halo density inferred from observational data exacerbates the problem. Even the smallest predicted inner density slope from simulations is still greater than that from observations. Many solutions have been suggested to solve the cusp-core problem (Del Popolo & Le Delliou 2017). Within the CDM framework of collisionless dark matter, the baryonic solutions focus on different mechanisms for energy exchange between baryons and dark matter to enable a flatter inner density (Navarro et al. 1996; Oh et al. 2011; Benítez-Llambay et al. 2019). Beyond the CDM framework, the self-interacting dark matter is proposed as a potential solution (Spergel & Steinhardt 2000; Rocha et al. 2013; Peter et al. 2013). The elastic scattering with a
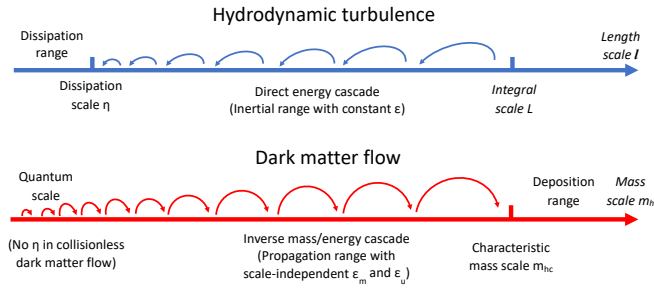
Figure 1. Schematic plot of the direct energy cascade in turbulence and the inverse mass and energy cascade in dark matter flow. Halos merge with single mergers to facilitate a continuous mass and energy cascade to large scales. Scale-independent mass flux ε_m and energy flux ε_u are expected for halos smaller than a characteristic mass scale (propagation range similar to the inertial range in turbulence). Mass cascaded from small scales is consumed to grow halos at scales above the characteristic mass (the deposition range similar to the dissipation range in turbulence), where mass and energy flux become scale-dependent (see Xu 2022a, for more details).

given cross-section facilitates the exchange of momentum and energy between dark matter particles and the formation of a flat core. Although the existence of dark matter is supported by numerous astronomical observations (Rubin & Ford 1970; Rubin et al. 1980), the nature and fundamental properties of dark matter are still a big mystery. No matter collisionless or self-interacting, some key questions remain open: what are the limiting length or density scales for dark matter if exist? what is the effect of self-interaction on these scales? what are the fundamental properties (particle mass, cross-section etc.) of dark matter? Answers to these questions would be critical for identifying and detecting dark matter.

In this paper, a cascade theory for dark matter flow is proposed to provide some useful insights, similar to the cascade in hydrodynamic turbulence. Both dark matter flow and turbulence are typical non-equilibrium systems involving energy cascade as a key mechanism to continuously release energy and maximize system entropy. To grasp the key idea, we first present the cascade in turbulence that has been well-studied for many decades (Taylor 1935, 1938; de Karman & Howarth 1938; Batchelor 1953). As shown in Fig. 1, turbulence consists of a collection of eddies (building blocks) on different length scale l that are interacting with each other. The classical picture of turbulence is an eddy-mediated energy cascade process, where kinetic energy of large eddies feeds smaller eddies, which feeds even smaller eddies, and so on to the smallest scale η where viscous dissipation is dominant. The direct energy cascade in turbulence can be best described by a poem (Richardson 1922):

"Big whirls have little whirls, That feed on their velocity;
And little whirls have lesser whirls, And so on to viscosity."

Despite the similarities, dark matter flow exhibits many different behaviors due to its collisionless and long-range interaction nature. First, unlike the turbulence that is incompressible on all scales, dark matter flow exhibits scale-dependent flow behaviors, i.e. a constant divergence flow on small scales and irrotational flow on large scales (Xu 2022f,g,i). Second, the long-range gravity requires a broad spectrum of halos to be formed to maximize the system entropy (Xu 2021c,d). In principle, halos of different mass can be grouped into groups of halos with the same mass m_h. Mass accretion facilitates a continuous mass and energy exchange between halos groups on different mass scale m_h, i.e. an inverse mass and energy cascade (Fig. 1). The rates of mass and energy cascade (ε_m and ε_u) have been shown to be independent of mass scale m_h (Xu 2021a,e).

The highly localized and over-dense halos are a major manifestation of nonlinear gravitational collapse (Neyman & Scott 1952; Cooray & Sheth 2002) and the building blocks of dark matter flow, a counterpart to "eddies" in turbulence. The halo-mediated inverse mass cascade is not present in turbulence, but exists as a local, two-way, and asymmetric process in dark matter flow (Xu 2021a). The net mass transfer proceeds in a "bottom-up" fashion from small to large mass scales (inverse cascade) to allow for structure formation. Halos pass their mass onto larger and larger halos, until halo mass growth becomes dominant over the mass propagation. From this description, mass cascade can be described by a similar poem with "eddies" (or "whirls") simply replaced by "halos":

"Little halos have big halos, That feed on their mass;
And big halos have greater halos, And so on to growth."

Energy cascade across halo groups is facilitated by the mass cascade and also a fundamental feature. Even on the halo scale, since halos are non-equilibrium objects, energy cascade should also play a role in the abundance and internal structure of halos. In this paper, we focus on the energy cascade, its evidence from galaxy rotation curves, and its critical role in halo internal structure and dark matter properties.

2   THE CONSTANT RATE OF ENERGY CASCADE

Particle-based N-body simulations are widely used to study the nonlinear gravitational collapse of dark matter (Peebles 1980). The simulation data for this work was generated from N-body simulations by Virgo consortium (Frenk et al. 2000; Jenkins et al. 1998). One way to determine the constant rate of energy cascade ε_u is from a cosmic energy equation for energy evolution of dark matter flow in expanding background (Irvine 1961; Layzer 1963; Xu 2022h),

$$\frac{\partial E_y}{\partial t} + H\left(2K_p + P_y\right) = 0, \tag{1}$$

which is a manifestation of energy conservation in expanding background. Here K_p is the specific (peculiar) kinetic energy, P_y is the specific potential energy in physical coordinate, $E_y = K_p + P_y$ is the total energy, $H = \dot{a}/a$ is the Hubble parameter ($Ht = 2/3$ for matter dominant universe), and a is the scale factor. In statistically steady state, Eq. (1) admits a linear solution of $K_p = -\varepsilon_u t$ and $P_y = 7/5\varepsilon_u t$ (see Fig. 2) such that ε_u can be found as,

$$\varepsilon_u = -\frac{K_p}{t} = -\frac{3}{2}\frac{u^2}{t} = -\frac{3}{2}\frac{u_0^2}{t_0} = -\frac{9}{4}H_0 u_0^2 \approx -4.6 \times 10^{-7}\frac{m^2}{s^3}, \tag{2}$$

where $u_0 \equiv u\left(t = t_0\right) \approx 354.6 km/s$ is the one-dimensional velocity dispersion of all dark matter particles and t_0 is the present time.

The constant ε_u represents the rate of energy cascade across different scales. The negative value $\varepsilon_u < 0$ reflects the direction (inverse) from small to large mass scales. Since baryons and dark matter are coupled together through gravitational interaction, the flow of baryonic matter should share the same rate of cascade that can be demonstrated by galaxy rotating curves (see Xu 2022l, Fig. 10). This work focus on the energy cascade in the flow of dark matter.

3   THE 2/3 AND -4/3 LAWS FOR ENERGY AND DENSITY

To develop statistical theory of dark matter flow on all scales, different statistical measures can be introduced including the correlation, structure, dispersion functions, and power spectrum for density, velocity and potential fields (Xu 2022f,g,i). Among different measures,
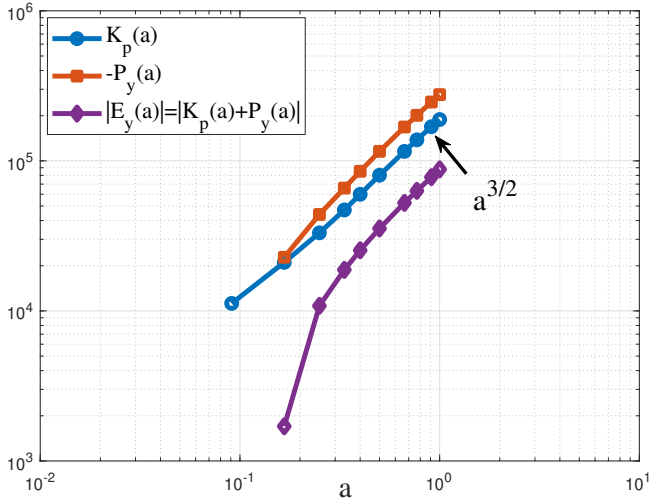
Figure 2. The time variation of kinetic and potential energies from N-body simulation. Both exhibit a power-law scaling with scale factor a, i.e. K_p and $P_y \propto a^{3/2} \propto \varepsilon_u t$. The proportional constant $\varepsilon_{\mathbf{u}}$ is estimated in Eq. (2).

Figure 3. Sketch of longitudinal and transverse velocities, where $\mathbf{u}_T$ and $\mathbf{u}'_T$ are transverse velocities at two locations $\mathbf{x}$ and $\mathbf{x}'$. u_L and u'_L are two longitudinal velocities.

structure functions are of particular interest that describes how energy is distributed and transferred across different length scales. For a pair of particles at two different locations $\mathbf{x}$ and $\mathbf{x}'$ with velocity $\mathbf{u}$ and $\mathbf{u}'$, the second order longitudinal structure function S_2^{lp} (pairwise velocity dispersion in cosmology terms) is defined as

$$S_2^{lp}(r,t) = \left\langle (\Delta u_L)^2 \right\rangle = \left\langle \left(u'_L - u_L \right)^2 \right\rangle, \tag{3}$$

where $u_L = \mathbf{u} \cdot \hat{\mathbf{r}}$ and $u'_L = \mathbf{u}' \cdot \hat{\mathbf{r}}$ are two longitudinal velocities. The distance $r \equiv |\mathbf{r}| = |\mathbf{x}' - \mathbf{x}|$ and the unit vector $\hat{\mathbf{r}} = \mathbf{r}/r$ (see Fig. 3). For a given scale r, all particle pairs with the same separation r can be identified in N-body simulation. The particle position and velocity data were recorded to compute the structure function in Eq. (3) by averaging over all pairs with the same r (i.e. a pairwise average).

In incompressible flow, the structure function has a small scale limit $\lim_{r \to 0} S_2^{lp} = 0$ because of $u_L \approx u'_L$ due to the viscous force. However, in dark matter flow, $\lim_{r \to 0} S_2^{lp} = 2u^2 \neq 0$ due to the collisionless nature (Xu 2022j), where u^2 is velocity dispersion in Eq. (2). The pair of particles with a sufficiently small r is more likely from the same halo, while different pairs can be from different halos. Kinetic energy of particle pairs on scale r includes contributions from both the relative motion of two particles and the motion of halos that particle pair resides in. The kinetic energy from the motion of halos is relatively same for different pairs. Kinetic energy involved in the energy cascade should be the part due to the relative motion.
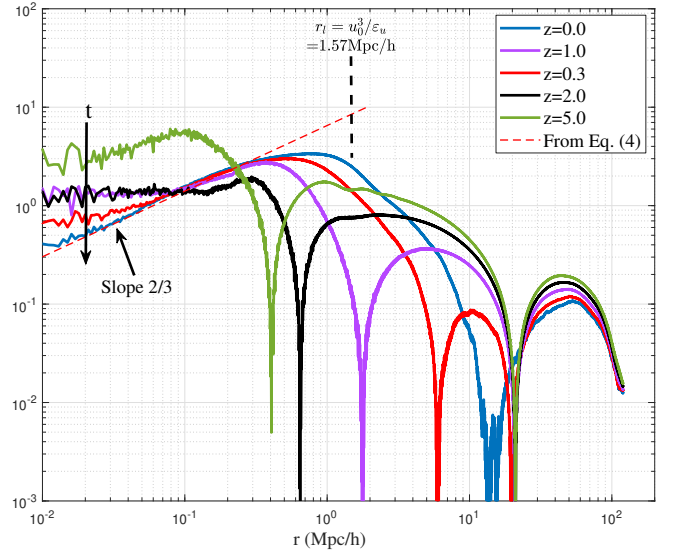
Figure 4. The variation of reduced second order structure function $S_2^{lp}(r)$ with comoving scale r at different redshift z. Structure function is normalized by the velocity dispersion u^2. A two-thirds law, i.e. $\propto (-\varepsilon_u)^{2/3} r^{2/3}$ can be clearly identified on small scale below a length scale $r_l = -u_0^3/\varepsilon_u$, where inverse energy cascade is established with a constant energy flux $\varepsilon_u < 0$. The model from Eq. (4) is also presented for comparison.

Since original pairwise dispersion $S_2^{lp}(r)$ includes the total kinetic energy on scale r, a reduced structure function $S_{2r}^{lp}(r) = S_2^{lp} - 2u^2$ can be introduced to take the common part out and include only the part from relative motion with the right limit $\lim_{r \to 0} S_{2r}^{lp} = 0$. This description indicates that $S_{2r}^{lp}(r)$ should be determined by and only by ε_u (m^2/s^3), gravitational constant G ($m^3/kg \cdot s^2$), and scale r. By a simple dimensional analysis, this reduced structure function must follow a two-thirds law, i.e. $S_{2r}^{lp}(r) \propto (-\varepsilon_u)^{2/3} r^{2/3}$.

Figure 4 plots the variation of S_{2r}^{lp} with scale r at different redshifts z from N-body simulations. The range $S_{2r}^{lp} \propto (-\varepsilon_u r)^{2/3}$ can be clearly identified below a critical length scale $r_l = -u_0^3/\varepsilon_u$. This range is formed due to the formation of halos and inverse energy cascade. On small scale, S_{2r}^{lp} (kinetic energy) should finally read

$$S_{2r}^{lp}(r) = a^{3/2} \beta_2^* (-\varepsilon_u)^{2/3} r^{2/3}, \tag{4}$$

where the proportional constant $\beta_2^* \approx 9.5$ can be found from Fig. 4. Since S_{2r}^{lp} represents the kinetic energy of relative motion on scale r, a different form of the two-thirds law (Eq. (4)) can be obtained. By introducing a typical velocity v_r on a given scale r,

$$v_r^2 = S_{2r}^{lp}(r) / \left(2^{2/3} \beta_2^* a^{3/2} \right), \tag{5}$$

the two-thirds law in Eq. (4) can be equivalently written as,

$$-\varepsilon_u = \frac{2v_r^2}{r} v_r = a_r v_r = \frac{2v_r^2}{r/v_r} = \frac{2v_r^3}{r}, \tag{6}$$

where a_r is the scale of acceleration. Equation (6) also describes the cascade of kinetic energy in the inner halo region ($r < r_s$, where r_s is the scale radius). The kinetic energy v_r^2 on scale r is cascaded to large scale during a turnaround time of $t_r = r/v_r$. Combining Eq. (6) with the virial theorem $Gm_r/r \propto v_r^2$ on scale r, we can easily obtain the typical mass m_r (enclosed within r), density ρ_r, velocity

v_r, and time t_r on scale r, all determined by ε_u, G, and r:

$$m_r = \alpha_r \varepsilon_u^{2/3} G^{-1} r^{5/3} \quad \text{and} \quad \rho_r = \beta_r \varepsilon_u^{2/3} G^{-1} r^{-4/3},$$
$$v_r \propto (-\varepsilon_u r)^{1/3} \quad \text{and} \quad t_r \propto (-\varepsilon_u)^{-1/3} r^{2/3}, \tag{7}$$

where α_r and β_r are two numerical constants. The predicted four-thirds law $\rho_r(r) \propto r^{-4/3}$ for mean density enclosed in scale r can be directly tested by data from galaxy rotation curves (see Fig. 5).

4 HALO DENSITY SLOPE AND MEAN RADIAL FLOW

On small scale, inner halo region is assumed to be fully virialized for Eq. (7) to be valid. A vanishing radial flow u_r is expected from the stable clustering hypothesis, i.e. no net stream motion in physical coordinate along radial direction (Mo et al. 2010). With $u_r \equiv 0$, there is no mass, momentum, and energy exchanges between different shells. However, halos are non-equilibrium dynamic objects, whose internal structure should be dependent on the radial flow. This relation we'll develop might be useful for core/cusp controversy.

Since halo density models often involve a scale radius r_s (the length scale of a halo), we may introduce a reduced spatial-temporal variable $x = r/r_s(t) = c(t)r/r_h(t)$, where $c \equiv c(t)$ is halo concentration and $r_h(t)$ is the virial size for halo of mass $m_h(t)$. Derivatives with respect to t and r can be derived using the chain rule,

$$\frac{\partial}{\partial t} = \frac{\partial}{\partial x}\frac{\partial x}{\partial t} = -\frac{x}{t}\frac{\partial \ln r_s}{\partial \ln t}\frac{\partial}{\partial x} \quad \text{and} \quad \frac{\partial}{\partial r} = \frac{\partial}{\partial x}\frac{\partial x}{\partial r} = \frac{1}{r_s}\frac{\partial}{\partial x}. \tag{8}$$

A general function $F(x)$ can be introduced such that the mass $m_r(r,t)$ enclosed in radius r and halo density $\rho_h(r,t)$ and can all be expressed in terms of function $F(x)$,

$$m_r(r,t) = m_h(t)\frac{F(x)}{F(c)},$$
$$\rho_h(r,t) = \frac{1}{4\pi r^2}\frac{\partial m_r(r,t)}{\partial r} = \frac{m_h(t)}{4\pi r_s^3}\frac{F'(x)}{x^2 F(c)}. \tag{9}$$

The time derivative of $\rho_h(r,t)$ can be obtained from Eq. (9),

$$\frac{\partial \rho_h(r,t)}{\partial t} = \frac{1}{4\pi r^2}\frac{\partial^2 m_r(r,t)}{\partial r \partial t}. \tag{10}$$

The mass continuity equation for a spherical halo simply reads,

$$\frac{\partial \rho_h(r,t)}{\partial t} + \frac{1}{r^2}\frac{\partial \left[r^2 \rho_h(r,t) u_r(r,t)\right]}{\partial r} = 0, \tag{11}$$

where $u_r(r,t)$ is the mean radial flow velocity. From Eqs. (10) and (11), the enclosed mass m_r is related to the radial flow as

$$\frac{\partial m_r(r,t)}{\partial t} = -4\pi r^2 u_r(r,t)\rho_h(r,t). \tag{12}$$

With m_r and ρ_h from Eq. (9), the radial flow u_r simply reads

$$u_r = -\frac{1}{4\pi r^2}\frac{\partial \ln m_r}{\partial \ln t}\frac{m_r(r,t)}{\rho_h(r,t)t} = -\frac{r_s(t)}{t}\frac{\partial \ln m_r}{\partial \ln t}\frac{F(x)}{F'(x)}. \tag{13}$$

While from Eq. (9) for m_r, we have

$$\frac{\partial \ln m_r}{\partial \ln t} = \frac{\partial \ln m_h}{\partial \ln t} - \frac{xF'(x)}{F(x)}\frac{\partial \ln r_s}{\partial \ln t} - \frac{cF'(c)}{F(c)}\frac{\partial \ln c}{\partial \ln t}. \tag{14}$$

Substituting into Eq. (13), the normalized radial flow u_h reads

$$u_h(x) = u_r\frac{t}{r_s} = \left[x\frac{\partial \ln r_s}{\partial \ln t} + \left(\frac{\partial \ln F(c)}{\partial \ln t} - \frac{\partial \ln m_h}{\partial \ln t}\right)\frac{F(x)}{F'(x)}\right]. \tag{15}$$

For fast growing halos in their early stage with a constant $c = 3.5$ and $r_s(t) \propto m_h(t) \propto t$ (Xu 2021b, 2022e), the cored density (pISO,

Einasto, etc.) leads to $u_h = 2x/3$, while NFW profile leads to $u_h = x/2$ (see Eqs. (15) and (19)). Taking the derivative in Eq. (15), the density slope γ can be obtained exactly as,

$$\gamma = \frac{\partial \ln \rho_h}{\partial \ln x} = \frac{\frac{\partial u_h}{\partial x} + \frac{\partial \ln m_r(r_s,t)}{\partial \ln t} - \frac{\partial \ln r_s}{\partial \ln t}}{\frac{\partial \ln r_s}{\partial \ln t} - \frac{u_h}{x}} - 2. \tag{16}$$

Clearly, the spatial variation of slope γ comes from the radial flow u_h, while the time variation of γ comes from $r_s(t)$ and $m_r(r_s,t)$ due to mass accretion. For fully virialized halos or the virialized inner core, we should have $u_h \equiv 0$ such that the asymptotic slope γ reads

$$\gamma = \frac{\partial \ln \rho_h}{\partial \ln x} = \frac{\partial \ln m_r(r_s,t)}{\partial \ln r_s} - 3. \tag{17}$$

On halo scale, energy cascade with a constant rate ε_u is valid for all scales $r \leqslant r_s$. Taking the enclosed mass $m_r(r_s)$ as the mass scale in Eq. (7), we found $m_r(r_s) \propto r_s^{5/3}$. For fully virialized halos with $u_h \equiv 0$, slope $\gamma = -4/3$ or a cuspy density $\rho_h(r) \propto r^{-4/3}$ can be obtained from Eq. (16). Therefore, fully virialized halos should have universal cuspy density profiles due to energy cascade. In other words, simulated halos might have different slope γ due to nonzero radial flow and different mass accretion rate (Eq. (16)). The baryonic feedback provides potential mechanisms to enhance the gradient of u_h (deformation rate) in Eq. (16)) and flatten the inner density. Finally, since $u_h(x = 0) \equiv 0$, there exists an asymptotic slope γ at $x = 0$ that is dependent on the local gradient of u_h around $x = 0$. Therefore, a better density profile (modified Einasto) can be proposed

$$\rho_h(r) = \rho_0 x^\gamma \exp\left(-\frac{2}{\alpha}x^\alpha\right),$$
$$F(x) = \Gamma\left(\frac{3+\gamma}{\alpha}\right) - \Gamma\left(\frac{3+\gamma}{\alpha}, \frac{2}{\alpha}x^\alpha\right). \tag{18}$$

Here ρ_0 and α are density and shape parameters and slope $\gamma < 0$.

5 TESTING -4/3 LAW AGAINST ROTATION CURVES

Next, the predicted four-thirds law in Eq. (7) ($\rho_r(r_s) \propto r_s^{-4/3}$) is tested against galaxy rotation curves that contain important information for dark matter halos. In practice, rotational curves can be first decomposed into contributions from different mass components. Model parameters for halo density (scale radius r_s and density scale ρ_0) are obtained by fitting to the decomposed rotation curve. Here we use three sources of galaxy rotation curves,

(i) SPARC (Spitzer Photometry & Accurate Rotation Curves) including 175 late-type galaxies (Lelli et al. 2016; Li et al. 2020);
(ii) DMS (DiskMass Survey) including 30 spiral galaxies (Martinsson et al. 2013);
(iii) SOFUE (compiled by Sofue) with 43 galaxies (Sofue 2016).

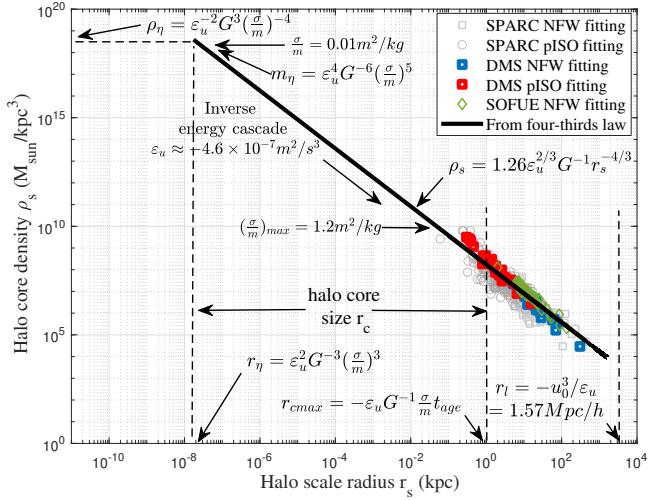For pseudo-isothermal (pISO) and NFW density models, we have

$$\rho_{pISO} = \frac{\rho_0}{1+x^2}, \quad F(x) = x - \arctan(x) \approx \frac{x^3}{3},$$
$$\rho_{NFW} = \frac{\rho_0}{x(1+x)^2}, \quad F(x) = \log(1+x) - \frac{x}{(1+x)} \approx \frac{x^2}{2}, \tag{19}$$

where ρ_0 is a density parameter. From Eq. (9), halo density at r_s is

$$\rho_h(r_s) = \rho_h(x=1) = \bar{\rho}_h\frac{c^3 F'(1)}{3F(c)} = \Delta_c \rho_{crit}\frac{c^3 F'(1)}{3F(c)}, \tag{20}$$

where $\bar{\rho}_h$ is the mean halo density. In this work, $\Delta_c = 200$ and critical density $\rho_{crit} = 3H_0^2/8\pi G = 10^{-26} kg/m^3$. Using Eqs. (19) and (20),

Figure 5. The predicted -4/3 law tested against actual data from galaxy rotation curves. Good agreement confirms the existence of inverse energy cascade with rate ε_u. The self-interacting dark matter model should modify the lowest size r_η and maximum density ρ_η determined by the cross-section σ/m, below which no coherent structure can exist. The largest possible core size r_{cmax} due to self-interaction is determined by the age of halos t_{age}. The largest scale r_l is determined by the velocity dispersion u_0 and ε_u.

concentration c can be obtained from fitted model parameter ρ_0. The mean density within r_s (density scale ρ_s) now reads

$$\rho_s(r_s) = \frac{m_r(r_s)}{4\pi r_s^3/3} = \frac{F(1)c^3}{F(c)}\bar{\rho}_h = \frac{F(1)c^3}{F(c)}\Delta_c\rho_{crit}, \quad (21)$$

Figure 5 presents the variation of typical density ρ_s with scale r_s obtained from three sources of galaxy rotation curves. The four-thirds law (Eq. (7)) is also plotted for comparison with coefficients $\beta_r = 1.26$ and $\alpha_r = 5.28$ obtained from these data. Clearly, dark matter halos obtained from rotation curves follow the four-thirds law across 6 order of size and density. Equivalently, the inner limiting density $\rho_h \propto r^{-4/3}$ for virialized halos with a vanishing radial flow is also confirmed by this plot using Eq. (17). Finally, this plot confirms the existence of a constant rate of cascade ε_u below the largest scale r_l. Other relevant quantities (density, pressure, energy etc.) on scale r_l are similarly determined by constants ε_u, G, and u_0 (Xu 2022k).

Finally, we can choose the circular velocity at r_s as the typical velocity $v_s = \sqrt{Gm_r(r_s)/r_s}$ such that $-\varepsilon_u = v_s^3/(\gamma_s r_s)$ (from Eq. (7)). Figure 6 presents the rate of energy cascade ε_u obtained from three sources of galaxy rotation curves with $\gamma_s = 6.83$. The dispersion in data might come from the spatial intermittence of energy cascade such that halos in different local environment may have slightly different ε_u (also see Xu 2022l). Dwarf galaxies tends to have smaller ε_u due to tidal stripping.

6 SCALES FOR SELF-INTERACTING DARK MATTER

To solve the core-cusp problem, the first option is the self-interacting dark matter (SIDM) model, where the cascade theory can be used to determine relevant scales. The cross-section σ/m of self-interaction should introduce additional scales r_η, ρ_η, and m_η (see Fig. 5), beyond which no structure can be formed due to self-interaction. These scales can be obtained by requiring at least one scatter per particle during the typical time t_r, i.e. $\rho_r(\sigma/m)v_r t_r = 1$ in Eq. (7). Combine this with the virial theorem and constant energy cascade in
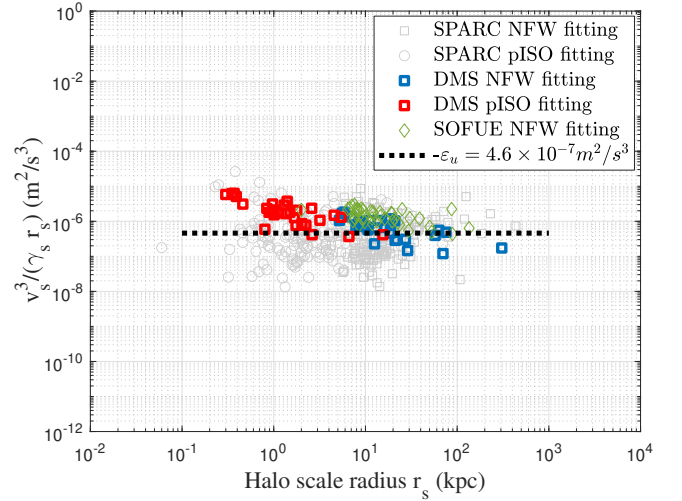
Figure 6. The constant rate of inverse energy cascade ε_u from galaxy rotation curve data. The dispersion in data might come from the spatial intermittence of energy cascade. Dwarf galaxy tends to have smaller ε_u. The flow of baryons shares the same rate of energy cascade (see Xu 2022l, for details).

Eq. (6), the limiting length r_η, density ρ_η, and mass m_η scales are determined by constants ε_u, G, and σ/m and shown in Fig. 5 (also see Xu 2022j, for details). In this plot, from galaxy rotation curves with a maximum core density around $\rho_\eta \approx 10^{10}M_{sun}/(kpc)^3$, we can safely estimate the upper limit of cross-section $\sigma/m \leqslant 1.2m^2/kg$ from expression for ρ_η. More stringent constraints were also obtained from Bullet Clusters (Robertson et al. 2016). High resolution rotation curves for dwarf galaxies should provide more information.

In addition, due to self-interaction, dark matter halo should have an isothermal core with a maximum core size r_{cmax} by requiring at least one scatter during the age of halos ($t_{age} \approx 1/H_0$), i.e. $\rho_r(\sigma/m)v_r t_{age} = 1$ such that (using Eq. (7))

$$\frac{r_{cmax}}{\sigma/m} = \varepsilon_u G^{-1}t_{age} = 100kpc\frac{kg}{m^2}. \quad (22)$$

For cross-section $\sigma/m = 0.01m^2/kg$ used in SIDM cosmological simulations (Rocha et al. 2013), halo core size is between r_η and the maximum core size $r_{cmax} \approx 1kpc$. In other words, maximum core size r_{cmax} formed from self-interaction (not any other mechanisms) can be used to identify the cross-section of postulated self-interaction.

In hydrodynamic turbulence, the smallest length scale $\eta = (v^3/\varepsilon)^{1/4}$ (Kolmogoroff 1941) is determined by the fluid viscosity v and rate of energy cascade ε. The kinetic energy is injected at large scale and cascaded down to small scales. Below scale η, structures (eddies) are destroyed by viscous force and kinetic energy is dissipated into heat to increase system entropy (Fig. 1). Here ε can be a variable manually controlled or adjusted by the rate of energy injection on large scale. For faster mixing, thinking about stirring the coffee-milk fluid harder (the larger ε), the scale η would be smaller and mixing would be faster on that scale. However, for dark matter flow in our universe, inverse (NOT direct) energy cascade is required for structure formation on large scales. The rate of energy cascade ε_u is a constant on small scales $r < r_l$, which should be a fundamental property of dark matter. Therefore, for self-interacting dark matter, it should be interesting and might be challenging to identify the potential mechanism on how the halo structure is generated on the smallest scale r_η along with the increasing system entropy, as this is exactly opposite to what we see in turbulence.
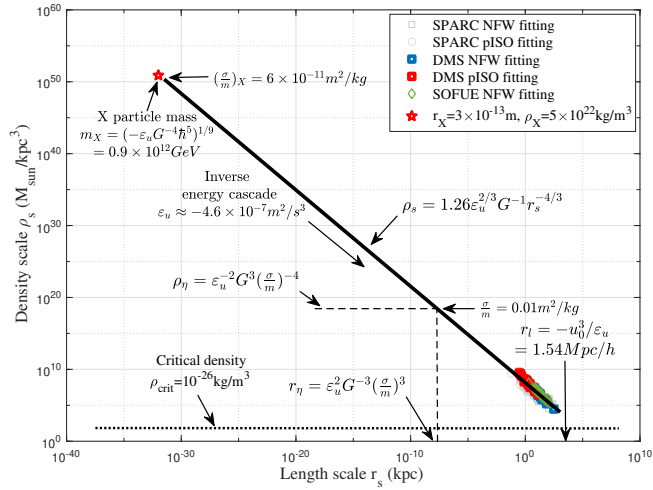
Figure 7. For fully collisionless dark matter, we may extend the predicted -4/3 law in Fig. 5 to the smallest scale where quantum effect can be important (red star). On this scale, dark matter particles properties are determined by three constants: ε_u, G, and Planck constant $\hbar$ (see Xu 2022j, for details).

7 SCALES FOR COLLISIONLESS DARK MATTER

Now let's consider the second option: dark matter is still fully collisionless with flat halo core formed by other possible mechanisms. In this scenario, due to the collisionless nature, the four-thirds law should extend from galaxy scale to the smallest scale where the quantum effect becomes important (Fig. 7). This extension is more than 30 orders in size, which hopefully allows us to predict the mass, size and properties of dark matter particles (the X particle) from three basic constants, i.e. ε_u, G, and Planck constant $\hbar$ (see Xu 2022j, for details). Two examples are the critical mass and length scales,

$$m_X \propto \left(-\frac{\varepsilon_u \hbar^5}{G^4}\right)^{\frac{1}{9}} \approx 10^{12} GeV, \quad r_X \propto \left(-\frac{G\hbar}{\varepsilon_u}\right)^{\frac{1}{3}} \approx 10^{-13} m. \quad (23)$$

If this is true, the constant ε_u might be an intrinsic property of dark matter with a similar origin as Planck constant $\hbar$ for two reasons:

(i) For fully collisionless dark matter, there exists a unique "symmetry" between position and velocity in phase space. At any given location, collisionless particles can have multiple values of velocity (multi-stream regime). Similarly, particles with same velocity can be found at different locations. This "symmetry" in phase space is not possible for any non-relativistic baryonic matter.

(ii) Due to the long-rang gravitational interaction, there exist fluctuations (uncertainty) not only in position ($\mathbf{x}$) and velocity ($\mathbf{v} = \dot{\mathbf{x}}$), but also in acceleration ($\mathbf{a} = \dot{\mathbf{v}}$), which provides a potential explanation for the origin of critical acceleration a_0 in MOND (modified Newtonian dynamics) (see Xu 2022k, for details).

With $\psi(x)$, $\varphi(p)$, and $\mu(a)$ as wave functions for position, momentum, and acceleration, we can write

$$\psi(x) = \frac{1}{\sqrt{2\pi\hbar}} \int_{-\infty}^{\infty} \varphi(p) \cdot e^{ip \cdot x/\hbar} \, dp \,,$$
$$\varphi(p) = \frac{1}{\sqrt{2\pi\mu_X}} \int_{-\infty}^{\infty} \mu(a) \cdot e^{ia \cdot p/\mu_X} \, da \,,$$
$$(24)$$

where constant $\mu_X = -m_X \varepsilon_u = 7.44 \times 10^{-22} kg \cdot m^2/s^3$ (also discussed in Xu 2022j). An energy scale $\sqrt{\hbar\mu_X} \approx 10^{-9} eV$ can be obtained for the possible dark radiation due to dark matter annihilation or decay. Here we have two pairs of conjugate variables i) position

x and momentum p, and ii) momentum p and acceleration a. By following the standard wave mechanics (will not repeat here), two uncertainty principles can be established for fluctuations of position, momentum, and acceleration for collisionless dark matter,

$$\sigma_x \sigma_p \geqslant \hbar/2 \quad \text{and} \quad \sigma_p \sigma_a \geqslant \mu_X/2. \quad (25)$$

More experiment data might be required to test this postulation.

8 CONCLUSIONS

Smalls scale challenges suggest some missing pieces in our current understandings of dark matter. A cascade theory for dark matter flow might provide extra insights. The energy cascade with a constant rate ε_u across different scales is a fundamental feature of dark matter flow. N-body simulation suggests a two-thirds law, i.e. the kinetic energy $v_r^2 \propto (\varepsilon_u r)^{2/3}$ on scale r. This is equivalent to a four-thirds law for density on the same scale, i.e. $\rho_r \propto \varepsilon_u^{2/3} G^{-1} r^{-4/3}$, which can be directly confirmed by data from galaxy rotation curves. By identifying key constants on relevant scales, limiting scales for collisionless (determined by ε_u, G, $\hbar$) or self-interacting dark matter (by ε_u, G, σ/m) might be obtained. On halo scale, based on the continuity equation, halo density is shown to be closely dependent on the radial flow and mass accretion. The asymptotic density slope $\gamma = -4/3$ can be obtained and fully virialized halos with a vanishing radial flow have a universal density profile. Simulated halos can have different limiting slopes due to finite radial flow and mass accretion, with a modified Einasto density profile proposed accordingly.

DATA AVAILABILITY

Two datasets for this article, i.e. a halo-based and correlation-based statistics of dark matter flow, are available on Zenodo (Xu 2022b,c), along with the accompanying presentation "A comparative study of dark matter flow & hydrodynamic turbulence and its applications" (Xu 2022a). All data are also available on GitHub (Xu 2022d).

REFERENCES

Batchelor G. K., 1953, The Theory of Homogeneous Turbulence. Cambridge University Press, Cambridge, UK
Benítez-Llambay A., Frenk C. S., Ludlow A. D., Navarro J. F., 2019, Monthly Notices of the Royal Astronomical Society, 488, 2387
Boylan-Kolchin M., Bullock J. S., Kaplinghat M., 2011, Monthly Notices of the Royal Astronomical Society: Letters, 415, L40
Boylan-Kolchin M., Bullock J. S., Kaplinghat M., 2012, Monthly Notices of the Royal Astronomical Society, 422, 1203
Bullock J. S., Boylan-Kolchin M., 2017, ARA&A, 55, 343
Cooray A., Sheth R., 2002, Physics Reports-Review Section of Physics Letters, 372, 1
Del Popolo A., Le Delliou M., 2017, Galaxies, 5, 17
Del Popolo A., Lima J. A. S., Fabris J. C., Rodrigues D. C., 2014, J. Cosmology Astropart. Phys., 2014, 021
Diemand J., Moore B., 2011, Advanced Science Letters, 4, 297
Famaey B., McGaugh S., 2013, in Journal of Physics Conference Series. p. 012001 (arXiv:1301.0623), doi:10.1088/1742-6596/437/1/012001
Flores R. A., Primack J. R., 1994, ApJ, 427, L1
Frenk C. S., White S. D. M., 2012, Annalen der Physik, 524, 507
Frenk C. S., et al., 2000, arXiv:astro-ph/0007362v1
Garrison-Kimmel S., Boylan-Kolchin M., Bullock J. S., Kirby E. N., 2014, Monthly Notices of the Royal Astronomical Society, 444, 222
Governato F., et al., 2010, Nature, 463, 203
Irvine W. M., 1961, Thesis, HARVARD UNIVERSITY

Jenkins A., et al., 1998, Astrophysical Journal, 499, 20

Klypin A., Kravtsov A. V., Valenzuela O., Prada F., 1999, The Astrophysical Journal, 522, 82

Kolmogoroff A. N., 1941, Comptes Rendus De L Academie Des Sciences De L Urss, 32, 16

Komatsu E., et al., 2011, ApJS, 192, 18

Kuzio de Naray R., Kaufmann T., 2011, Monthly Notices of the Royal Astronomical Society, 414, 3617

Layzer D., 1963, Astrophysical Journal, 138, 174

Lelli F., McGaugh S. S., Schombert J. M., 2016, AJ, 152, 157

Li P., Lelli F., McGaugh S., Schombert J., 2020, ApJS, 247, 31

Martinsson T. P. K., Verheijen M. A. W., Westfall K. B., Bershady M. A., Andersen D. R., Swaters R. A., 2013, A&A, 557, A131

McGaugh S. S., Schombert J. M., Bothun G. D., de Blok W. J. G., 2000, Astrophysical Journal, 533, L99

McKeown D., et al., 2022, MNRAS, 513, 55

Milgrom M., 1983, Astrophysical Journal, 270, 365

Mo H., van den Bosch F., White S., 2010, Galaxy formation and evolution. Cambridge University Press, Cambridge

Moore B., Ghigna S., Governato F., Lake G., Quinn T., Stadel J., Tozzi P., 1999, The Astrophysical Journal, 524, L19

Navarro J. F., Eke V. R., Frenk C. S., 1996, MNRAS, 283, L72

Navarro J. F., Frenk C. S., White S. D. M., 1997, Astrophysical Journal, 490, 493

Navarro J. F., et al., 2010, Monthly Notices of the Royal Astronomical Society, 402, 21

Neyman J., Scott E. L., 1952, Astrophysical Journal, 116, 144

Oh S.-H., Brook C., Governato F., Brinks E., Mayer L., de Blok W. J. G., Brooks A., Walter F., 2011, AJ, 142, 24

Peebles P. J. E., 1980, The Large-Scale Structure of the Universe. Princeton University Press, Princeton, NJ

Peebles P. J. E., 1984, ApJ, 284, 439

Perivolaropoulos L., Skara F., 2022, New Astronomy Reviews, 95, 101659

Peter A. H. G., Rocha M., Bullock J. S., Kaplinghat M., 2013, MNRAS, 430, 105

Richardson L. F., 1922, Weather Prediction by Numerical Process. Cambridge University Press, Cambridge, UK

Robertson A., Massey R., Eke V., 2016, Monthly Notices of the Royal Astronomical Society, 465, 569

Rocha M., Peter A. H. G., Bullock J. S., Kaplinghat M., Garrison-Kimmel S., Oñorbe J., Moustakas L. A., 2013, Monthly Notices of the Royal Astronomical Society, 430, 81

Rubin V. C., Ford W. K., 1970, Astrophysical Journal, 159, 379

Rubin V. C., Ford W. K., Thonnard N., 1980, Astrophysical Journal, 238, 471

Sofue Y., 2016, Publications of the Astronomical Society of Japan, 68

Spergel D. N., Steinhardt P. J., 2000, Phys. Rev. Lett., 84, 3760

Spergel D. N., et al., 2003, ApJS, 148, 175

Swaters R. A., Madore B. F., van den Bosch F. C., Balcells M., 2003, Astrophys. J., 583, 732

Taylor G. I., 1935, Proceedings of the royal society A, 151, 421

Taylor G. I., 1938, Proceedings of the Royal Society of London Series a-Mathematical and Physical Sciences, 164, 0015

Xu Z., 2021a, arXiv e-prints, p. arXiv:2109.09985

Xu Z., 2021b, arXiv e-prints, p. arXiv:2109.12244

Xu Z., 2021c, arXiv e-prints, p. arXiv:2110.03126

Xu Z., 2021d, arXiv e-prints, p. arXiv:2110.09676

Xu Z., 2021e, arXiv e-prints, p. arXiv:2110.13885

Xu Z., 2022a, A comparative study of dark matter flow & hydrodynamic turbulence and its applications, doi:10.5281/zenodo.6569901, http://dx.doi.org/10.5281/zenodo.6569901

Xu Z., 2022d, Dark matter flow dataset, doi:10.5281/zenodo.6586212, https://github.com/ZhijieXu2022/dark_matter_flow_dataset

Xu Z., 2022b, Dark matter flow dataset Part I: Halo-based statistics from cosmological N-body simulation, doi:10.5281/zenodo.6541230, http://dx.doi.org/10.5281/zenodo.6541230

Xu Z., 2022c, Dark matter flow dataset Part II: Correlation-based statistics from cosmological N-body simulation, doi:10.5281/zenodo.6569898, http://dx.doi.org/10.5281/zenodo.6569898

Xu Z., 2022e, arXiv e-prints, p. arXiv:2201.12665

Xu Z., 2022f, arXiv e-prints, p. arXiv:2202.00910

Xu Z., 2022g, arXiv e-prints, p. arXiv:2202.02991

Xu Z., 2022h, arXiv e-prints, p. arXiv:2202.04054

Xu Z., 2022i, arXiv e-prints, p. arXiv:2202.06515

Xu Z., 2022j, arXiv e-prints, p. arXiv:2202.07240

Xu Z., 2022k, arXiv e-prints, p. arXiv:2203.05606

Xu Z., 2022l, arXiv e-prints, p. arXiv:2203.06899

de Blok W. J. G., 2010, Adv. Astron., 2010, 789293

de Blok W. J. G., Bosma A., 2002, A&A, 385, 816

de Blok W. J. G., Bosma A., McGaugh S., 2003, Monthly Notices of the Royal Astronomical Society, 340, 657

de Karman T., Howarth L., 1938, Proceedings of the Royal Society of London Series a-Mathematical and Physical Sciences, 164, 0192